Applied Geochemistry 81 (2017) 53–62

Contents lists available at ScienceDirect

Applied Geochemistry

journal homepage: www.elsevier.com/locate/apgeochem

Rate equations for modeling carbon dioxide sequestration in basalt

Ryan M. Pollyea*, J. Donald Rimstidt

Department of Geosciences, Virginia Polytechnic Institute and State University, Blacksburg VA 24061, USA

ARTICLE INFO

Article history:
Received 23 November 2016
Received in revised form
30 March 2017
Accepted 31 March 2017
Available online 2 April 2017

Editorial handling by Prof. M. Kersten.

Keywords:
CO_2 sequestration
TOUGHREACT models
Glassy basalt rate equation
Crystalline basalt rate equation

ABSTRACT

Dissolution rate equations are developed from published data for glassy and crystalline basalt to predict the silica release flux (J_{Si}) as a function of hydrogen ion activity ($2 < pH < 12$) and temperature ($0° < T < 100 °C$). For glassy basalt the silica flux is

$$J_{Si} = (5.00 \times 10^2)e^{\left(\frac{-39700}{R}\right)\frac{1}{T}}a_{H^+}^{1.01} + (5.26 \times 10^{-5})e^{\left(\frac{-38400}{R}\right)\frac{1}{T}}a_{H^+}^{-0.258}$$

and for crystalline basalt the silica flux is

$$J_{Si} = (7.40)e^{\left(\frac{-40100}{R}\right)\frac{1}{T}}a_{H^+}^{0.680} + (8.67 \times 10^{-7})e^{\left(\frac{-32900}{R}\right)\frac{1}{T}}a_{H^+}^{-0.286}.$$

These rate equations are implemented in TOUGHREACT to simulate a CO_2 saturated solution reacting with glassy and crystalline basalt in batch and semibatch reactors. The crystalline basalt models are compared with a more complex basalt representation comprising a composite mixture of olivine, plagioclase and pyroxene dissolution rates. Results show that numerical models based on the newly developed rate equations make reasonable predictions. Batch reactor models initially contained a solution spiked with CO_2. These models showed relatively rapid CO_2 consumption followed by cessation of the reaction with the glassy and crystalline basalt after the CO_2 was exhausted and a terminal pH near eight. The composite basalt model was less successful because the plagioclase continued to react after the CO_2 was exhausted causing the pH to rise to an unreasonably high value near 12. Semibatch reactor models containing a solution continuously supplied with CO_2 showed relatively rapid CO_2 consumption until all basalt was consumed. Complete semibatch reaction produced a sodium and bicarbonate rich solution with a pH near eight for all three basalt compositions.

1. Introduction

The suitability of basalt reservoirs for carbon capture and sequestration (CCS) is being tested on the basis of favorable CO_2-water-rock geochemical reactions that result in permanent CO_2 isolation through mineral trapping (Matter et al., 2016; Bacon et al., 2014; Schaef et al., 2013; Gysi and Stefánsson, 2011; Matter and Kelemen, 2009; McGrail et al., 2017). The motivation for CCS in basalt is largely attributable to the relatively high CO_2 storage potential within both onshore and offshore basalt formations. For example, McGrail et al. (2006) estimate CO_2 storage potential in the Columbia River Basalt Group in the northwestern United States to be as high as 100 Gt CO_2, and studies by Goldberg et al. (2008, 2010) suggest that offshore basalt formations within the Juan de Fuca plate and Central Atlantic Magmatic Province hold potential for CO_2 disposal on comparable scales. On a global basis, perhaps the most significant opportunity for CCS in mafic reservoirs is within India's Deccan Traps, where CO_2 storage estimates are on the order of 150 Gt (Jayaraman, 2007), and the demand for coal-fired electricity is driven by rapid economic growth.

The premise motivating CCS in mafic reservoirs is that CO_2 dissolution in water produces carbonic acid, which provides hydrogen ions for basalt dissolution and bicarbonate ions for carbonate precipitation. The overall dissolution rate of the basalt governs cation availability and pH in the CO_2-water-basalt system and exerts first-order control on the mineral trapping potential of the reservoir. The first step in this process involves CO_2 dissolution to produce carbonic acid, which dissociates to bicarbonate and hydrogen ions:

$$CO_2 + H_2O = H_2CO_3 = H^+ + HCO_3^- \quad (1)$$

In the next step, the hydrogen ions promote the dissolution of the basalt. For Icelandic basalts considered in this paper, the

* Corresponding author.
E-mail address: rpollyea@vt.edu (R.M. Pollyea).

http://dx.doi.org/10.1016/j.apgeochem.2017.03.020
0883-2927/

generalized reaction based on the basalt composition from Oelkers and Gislason (2001) and Gudbrandsson et al. (2011) is:

$$\begin{aligned} &SiAl_{0.358}Fe_{0.190}Mg_{0.281}Ca_{0.264}Na_{0.079}K_{0.008}O_{3.315} + 2.630H^+ \\ &\quad + 0.685H_2O \\ &\quad = H_4SiO_4 + 0.358Al^{3+} + 0.190Fe^{2+} + 0.281Mg^{2+} \\ &\qquad + 0.264Ca^{2+} + 0.079Na^+ + 0.008K^+. \end{aligned} \tag{2}$$

At higher pH the aluminum hydrolyzes to form hydroxy species resulting in a proportionally lower consumption of hydrogen ions. In the final step, the divalent cations (Ca^{2+}, Mg^{2+}, and Fe^{2+}) from the dissolved basalt combine with bicarbonate and carbonate ions to precipitate carbonate minerals and release additional hydrogen ions into solution, e.g.,

$$Mg^{2+} + HCO_3^- = MgCO_3(s) + H^+. \tag{3}$$

In addition, the Si and Al from the basalt precipitates into clay minerals (e.g., illite and montmorillonite) and these reactions also produce hydrogen ions, which contribute to further basalt dissolution (Gysi and Stefánsson, 2012).

In recent years, several modeling studies and small-scale field experiments have shown that CO_2 sequestration in basalt reservoirs may be feasible despite significant levels of reservoir heterogeneity. For example, industrial-scale CO_2 sequestration has been tested in low-volume basalt reservoirs using Monte Carlo numerical modeling methods, which show that permeability heterogeneity strongly influences reservoir injectivity; however, the confinement potential is favorable over time-scales needed for mineralization (Pollyea et al., 2014; Pollyea and Fairley, 2012). Additionally, small-scale basalt sequestration field experiments have been undertaken at the Wallula Basalt Sequestration Pilot Project in southeastern Washington, USA (McGrail et al., 2017), and the CarbFix Project at Hellisheidi geothermal power plant in southwest Iceland (Matter et al., 2016; Gislason et al., 2010). While these projects are similar in their approach to carbon isolation through CO_2-water-rock mineralization reactions, the field implementation in each project differs in the delivery of CO_2. At the Wallula site, 1000 metric tons of CO_2 was injected in the supercritical (sc) phase in August 2013, and analysis of post-injection sidewall cores indicate that carbonate mineral precipitation was widespread in the injection zone (McGrail et al., 2017). At the CarbFix field site, two CO_2 injections were undertaken in 2012 (175 tons and 73 tons) to test the novel CO_2 delivery mechanism in which CO_2 and water are co-injected while keeping CO_2 concentration in the injected fluid below the solubility limit (Matter et al., 2016). This injection approach minimizes both degassing potential and buoyancy driven fluid flow, thus permitting CO_2 injections at moderate depths (400–800 m), where pure CO_2 would be subcritical (Sigfusson et al., 2015). During the CarbFix injections, the CO_2 was spiked with radioactive ^{14}C to quantify the *in situ* mass conversion of CO_2 to carbonate minerals, and results indicate that over 95% of the injected CO_2 mass was isolated within 2 years of the injections (Matter et al., 2016).

The promising results from the Wallula and CarbFix demonstration sites strongly motivate continued research towards understanding the CO_2-water-basalt system for CCS applications. Consequently, there is increasing demand for simulation tools that can be readily implemented for modeling the behavior of high P_{CO2} systems. As a result, the purpose of this paper is to report rate equations that can be used to predict rates of CO_2 consumption by reactions with crystalline or glassy basalt. We fit published silica release rates for glassy and crystalline Icelandic basalt to equations that predict dissolution rates as a function of pH and temperature. The application of these glassy and crystalline basalt dissolution equations is illustrated in batch (closed) and semibatch (fixed P_{CO2}) reactor simulations using the TOUGHREACT numerical simulator for non-isothermal multi-phase reactive transport (Xu et al., 2014). Input records for the implementation of these rate models are presented as Supplemental Information (Tables S1–S2).

2. Methods

2.1. Rate equations

Published experimental values of the silica release flux (J_{Si}) from crystalline and glassy Icelandic basalt samples were tabulated along with temperature and pH (Supplemental Information, Tables S3 and S4). For glassy basalt, there are 135 data (Flaathen et al., 2010; Gislason and Oelkers, 2003; Oelkers and Gislason, 2001; Wolff-Boenisch et al., 2004a) and for crystalline basalt there are 26 data (Gudbrandsson et al., 2011).

The silica release flux from dissolving basalt is primarily controlled by pH and temperature.

$$J_{Si} = k a_{H^+}^n = \left(A e^{-1000E_a} \Big/ RT\right) a_{H^+}^n. \tag{4}$$

In Equation (4), the activation energy (E_a) is commonly reported in kJ mol^{-1}, and we retain this unit convention here. As a result, E_a is scaled by the conversion factor 1000 J per kJ in order to maintain internal consistency with the gas constant (R), which has units of J mol^{-1} K^{-1}. See Table 1 for an explanation of the notation used in this paper. This equation can be linearized by a log transformation.

$$\log J_{Si} = \log k + n \log a_{H^+} = \log A - \frac{1000E_a}{2.303R}\left(\frac{1}{T}\right) - npH \tag{5}$$

The generalized form of this equation has three fitting parameters (a, b and c).

$$\log J_{Si} = a + \frac{b}{T} + cpH \tag{6}$$

Multiple linear regression modeling, using the JMP10 (SAS Institute Inc.) program, was applied to each data set to obtain values for a, b and c. Prior to regression analysis, the datasets were normalized to geometric surface area. Partial regression graphs, shown in Supplemental Information (Figs. S1–S4), were used to visualize the contribution of each independent variable to the overall fit (Moya-Laraño and Corcobado, 2008; Velleman and Welsch, 1981). These graphs plot the residuals of the dependent variable versus the residuals of each independent variable. The slope of the line on each graph equals the regression coefficient for that variable so that a steep slope means that the independent variable strongly influences the dependent variable. Inspection of the data showed a minimum in $\log J_{Si}$ near pH 6 for both glassy and crystalline basalt but no evidence for a rate plateau in the near neutral pH region. As a result, the data sets were divided at pH 6 fit to separate equations to get the dissolution flux for pH < 6 ($J_{<6Si}$) and for pH > 6 ($J_{>6Si}$). The rate equation for the entire pH range (2 < pH < 12) was constructed by summing the antilog transformation of the low and high pH equations ($J_{Si} = J_{<6Si} + J_{>6Si}$).

For use in TOUGHREACT, the rate equations from the regression models must be recast into the format used in Palandri and Kharaka (2004). This format is based on the idea that the overall rate is the sum of parallel, independent reaction rates. For reactions affected by only pH and temperature, the overall rate constant is calculated by summing the terms of following equation:

Table 1
Notation used in this paper.

A	pre-exponential in Arrhenius equation, mol/m^2 sec
a, b, c	fitted parameters determined by the regression model
a_i	activity of species i
$E_a^{H(NU, OH)}$	activation energy for acid, neutral, or base reaction, kJ/mol
J_{Si}	overall silica dissolution flux ($J = J_{<6Si} + J_{>6Si}$), mol/m^2 sec
$J_{<6Si}$	silica dissolution flux for pH < 6, mol/m^2 sec
$J_{>6Si}$	silica dissolution flux for pH > 6, mol/m^2 sec
k	rate constant, mol/m^{2}sec
$k_{25}^{H\ (NU,OH)}$	rate constant at 25 °C for acid, neutral, or base reaction, mol/m^{2}sec
K_i	solubility equilibrium constant for substance i
$n_{H\ (OH)}$	reaction order for hydrogen (or hydroxide) ions
pH	−log a_{H+}
R	gas constant, 8.314 J/mol K
R^2	coefficient of determination for the regression model
T	temperature, °C or K
x_i	mole fraction of substance i

$$k = k_{25}^{nu} exp\left[\frac{-E_a^{nu}}{R}\left(\frac{1}{T}-\frac{1}{298.15}\right)\right] + k_{25}^{H} exp\left[\frac{-E_a^{H}}{R}\left(\frac{1}{T}-\frac{1}{298.15}\right)\right] a_H^{n_H} + k_{25}^{OH} exp\left[\frac{-E_a^{OH}}{R}\left(\frac{1}{T}-\frac{1}{298.15}\right)\right] a_{OH}^{n_{OH}}, \tag{7}$$

To implement Equation (7) in TOUGHREACT, E_a is entered in units of kJ mol^{-1}, and the units are internally converted for consistency with R. The first term in Equation (7) predicts the dissolution rate for the pH independent reaction of a solid with pure water at near neutral pH. For the present study, this term is set to zero because the glassy and crystalline basalt do not show a near neutral rate plateau. The second term represents the reaction with hydrogen ions at low pH and the third term represents the reaction with hydroxide ions at high pH. These latter terms are implemented in the present study to account for pH dependence in the rate equations for glassy and crystalline basalt.

In order to populate Equation (7) using results from the regression models (Table 4), the a, b and c parameters from Equation (6) were converted to $k_{25}^{H(or\ OH)}$, $E_a^{H(or\ OH)}$ and $n_{H(or\ OH)}$ using the following relationships. The a parameter of the regression model is used to find $k_{25}^{H(and\ OH)}$. The pre-exponential ($A = 10^a$) in the rate equation is the rate constant at infinite temperature, which means that the a parameter from the regression model equals the logarithm of the rate constant at infinite temperature. This A term can be recast in terms of the rate constant at 25 °C.

$$J_{Si} = \left(k_{25^\circ} e^{\frac{-1000E_a}{R}\left(\frac{1}{T}-\frac{1}{298}\right)}\right) a_{H^+}^n \tag{8}$$

If this equation is log transformed and parsed in the following way, the $\log k_{25}^{H(or\ OH)}$ term can be isolated.

$$\begin{aligned} logJ_{Si} &= logk_{25^\circ} - \frac{1000E_a}{2.303R}\left(\frac{1}{T}-\frac{1}{298}\right) + nloga_{H^+} \\ &= logk_{25^\circ} - \frac{1000E_a}{2.303R}\left(\frac{1}{T}\right) + \frac{1000E_a}{2.303R}\left(\frac{1}{298}\right) + nloga_{H^+} \\ &= logk_{25^\circ} + \frac{1000E_a}{2.303(R\ 298)} - \frac{1000E_a}{2.303R}\left(\frac{1}{T}\right) + nloga_{H^+} \end{aligned} \tag{9}$$

This shows that the rate constant at 25 °C is related to the rate constant at infinite temperature as follows:

$$\begin{aligned} logA &= logk_{25^\circ} + \frac{1000E_a}{2.303R(298)} \\ logk_{25^\circ} &= logA - \frac{1000E_a}{2.303R(298)} = logA - \frac{1000E_a}{5.706} \end{aligned} \tag{10}$$

The b parameter of the regression model gives the values of $E_a^{H(and\ OH)}$,

$$E_a = \frac{2.303Rb}{1000}. \tag{11}$$

The c terms from the regression model gives the reaction orders for H^+ and OH^- ($n_{H(andOH)}$),

$$\text{pH} < 6:\ n_H = c \text{ and pH} > 6:\ n_{OH} = -c. \tag{12}$$

2.2. TOUGHREACT simulations

In order to evaluate the effectiveness of the rate equations presented in Section 2.1, six numerical simulations were developed using TOUGHREACT v3.2-OMP (Xu et al., 2014). These simulations implement the glassy basalt and crystalline basalt using the rate equations developed in this study. Because the crystalline basalt model simulates whole rock dissolution, this study also implements a composite basalt model, in which dissolution is modeled on the basis of individual rate equations for plagioclase, pyroxene, and olivine. For this composite basalt reactor, the volumetric proportion of each mineral phase is determined on the basis of Gudbrandsson et al. (2011), in which plagioclase is 41.3 vol%, pyroxene is 34.0 vol%, olivine is 15.8 vol%, and the remaining 8.9 vol% is non-reactive mineral volume. For the composite basalt models, plagioclase solubility is represented as labradorite ($An_{70}Ab_{30}$), pyroxene solubility is represented as the solid solution $Di_{45}Hd_{25}En_{19}Fs_{11}$ (Stefánsson, 2001), and olivine solubility is represented as forsterite. The kinetic dissolution rates for plagioclase, pyroxene, and olivine are based on labradorite, augite, and forsterite, respectively, using rate equations in Palandri and Kharaka (2004). The composite basalt representation is a more traditional formulation for reactive transport modeling, and has been implemented in basalt systems by Aradóttir et al. (2012a) to simulate reactive transport during CO_2 injections at the CarbFix site. In the remainder of this study, "glassy" and "crystalline" basalt rates refer to the dissolution rate equations developed in Section 2.1, and "composite" basalt refers to the model comprising individual dissolution rates for labradorite, forsterite, and augite.

Each of these three solid compositions (glassy, crystalline, and composite basalt) was reacted under two scenarios: (1) a batch reactor initially spiked with carbonic acid and then closed for all components and (2) a semibatch reactor continually open to CO_2 addition, but closed for all other components. Each simulation predicts the behavior of the solution and basalt in a 1 m × 1 m × 1 m grid cell packed with 1 mm diameter grains with 50% porosity. This configuration results in an initial reactive surface area of 6000 m^2/m^3 for the glassy and crystalline basalt reactors, and this surface area is scaled for the composite basalt reactor on the basis of mineral vol%. The initial water composition for the batch reactor simulations represents deionized water in equilibrium with 0.2 MPa (2 bar) P_{CO2} at 25 °C and 2.5 MPa fluid pressure and no more CO_2 was added to the reactor after this initial spike. This represents a one time injection of a slug of CO_2 saturated water into basalt. In contrast, the carbonic acid concentration in the semibatch reactor simulations was continually in equilibrium with a P_{CO2} of 0.2 MPa (2 bar) at 25 °C and 2.5 MPa fluid pressure. This

exemplifies a basalt subject to CO_2 outgassing (Gizaw, 1996) or during CCS where an advancing CO_2 plume provides a constant supply of free phase CO_2 (McGrail et al., 2014). Each run modeled the behavior for 1,000,000 years at time increments (Δt) of 10 days, which provided sufficient time for complete basalt dissolution in the semibatch reactor scenarios.

In order to account for the effect of chemical potential on dissolution rate, we estimated equilibrium solubility constants for the glassy and crystalline basalts. Several methods have been proposed to estimate solubility constants of glass phases. For example, Gislason and Oelkers (2003) and Wolff-Boenisch et al. (2004a) estimate the solubility constant for basalt glass using hydrated volcanic glass as a proxy. For this study, the glassy basalt solubility constant was estimated using the method of Paul (1977), following the lead of Techer et al. (2001) and Aradóttir et al. (2012b). According to this approach, the solubility of a glass phase is approximated by the weighted sums of the component oxide solubility constants and oxide mole fractions as given by:

$$logK_{glass} = \sum_i x_i logK_i + \sum_i x_i logx_i \quad (13)$$

where, K_{glass} is the equilibrium solubility constant for a glass comprising x mole fraction of oxide i with a corresponding solubility constant of K_i. The mole fraction of component oxides used for this calculation are given in Table 2. The log K_{glass} values given in Table 3 were computed for temperature between 0 and 100 °C using thermodynamic data from the Thermodemm v.1.10 database (Blanc et al., 2012). These calculations assume that all iron exists as FeO, and TiO_2, MnO, and P_2O_5 are neglected because they are of minimal interest in CCS modeling and comprise less than 2 wt percent of the basalt (Aradóttir et al., 2012b). Icelandic crystalline basalt has essentially the same composition as glassy basalt (Gudbrandsson et al., 2011). Based on the observation that the solubility of quartz is about one order of magnitude lower than the solubility of pure silica glass, the solubility equilibrium constants for the crystalline basalt were estimated to be one order of magnitude lower than the corresponding glass phase (Table 3). The solubility constants for each mineral in the composite basalt are given in Table 3.

The input records needed to implement the kinetic dissolution rates in TOUGHREACT for glassy and crystalline basalt are presented as the Supplemental Information for this paper (Tables S1–S2). The dissolution equation is normalized to Si for both glassy and crystalline basalt (Equation (2)), and written in terms of the primary aqueous species used in the Thermodemm v1.10 (Blanc et al., 2012) thermodynamic database, which is freely available in the format required for TOUGHREACT. The rate parameters for each basalt reactor model are given in Table 5. The complete list of initial molal concentrations for primary aqueous species within each reactor simulation is presented in Table 6, and a combined table presenting both the primary aqueous species and aqueous complexes (secondary species) is presented as supplementary material (Table S5). For each reactor simulation, a simplified set of six alteration products can precipitate on the basis of local equilibrium: calcite, siderite, magnesite, amorphous silica, illite ($K_{0.85}Fe_{0.25}Al_{2.35}Si_{3.4}O_{10}(OH)_2$), and montmorillonite ($Ca_{0.17}Mg_{0.34}Al_{1.66}Si_4O_{10}(OH)_2$). This simplified alteration assemblage was selected in order to provide simulation results that can be interpreted on the basis of both physical intuition and comparative analysis between the crystalline and composite basalt reactors. In addition, zeolite phases are known alteration products in basalt weathering (Gysi and Stefánsson, 2011). As result, a second set of batch and semi-batch reactor simulations was completed in which sodium-bearing heulandite is added to the assemblage of alteration products.

Table 2
Oxide composition of glassy basalt.

Oxide	Weight %[a]	Mole fraction
SiO_2	48.12	0.504
Al_2O_3	14.62	0.090
FeO[b]	10.92	0.096
MgO	9.08	0.142
CaO	11.84	0.133
Na_2O	1.97	0.020
K_2O	0.29	0.002

[a] As reported by Oelkers and Gislason (2001).
[b] All iron reported as Fe(II).

Table 3
Log K for glassy and crystalline basalt and the minerals in the composite basalt.

	0 °C	25 °C	60 °C	100 °C
Glass[a]	10.581	9.337	7.910	6.608
Crystalline[b]	9.581	8.337	6.910	5.608
Forsterite[c]	32.130	28.604	24.586	20.958
Plagioclase[d]	24.014	20.062	15.325	10.893
Pyroxene[e]	11.680	10.450	8.920	7.580

[a] Calculated by Eq. (13).
[b] Assumed one order of magnitude lower than glassy basalt.
[c] Values from Thermodemm V1.10 database (Blanc et al., 2012).
[d] Log K for $An_{70}Ab_{30}$ from Stefánsson (2001).
[e] Log K for $Di_{45}Hd_{25}En_{19}Fs_{11}$ from Stefánsson (2001).

3. Results

3.1. Rate equations

The results of the regression models are given in Table 4. Data for both the glassy and crystalline basalts are evenly distributed between low and high pH. Based on the range of the independent variables (pH and T) used in the models we suggest that the rate equations based on these fits are suitable for modeling $0 < T < 100$ °C and $2 < \text{pH} < 12$. The silica dissolution fluxes predicted by these rate equations are illustrated in Fig. 1. For glassy basalt the rate equation is

$$J_{Si} = \left(5.00 \times 10^2\right) e^{\left(\frac{-39700}{R}\right)\frac{1}{T}} a_{H^+}^{1.01} + \left(5.26 \times 10^{-5}\right) e^{\left(\frac{-38400}{R}\right)\frac{1}{T}} a_{H^+}^{-0.258} \quad (14)$$

and the rate equation for crystalline basalt is

$$J_{Si} = (7.40) e^{\left(\frac{-40100}{R}\right)\frac{1}{T}} a_{H^+}^{0.680} + \left(8.67 \times 10^{-7}\right) e^{\left(\frac{-32900}{R}\right)\frac{1}{T}} a_{H^+}^{-0.286} \quad (15)$$

In Equations (14) and (15), the E_a for low and high pH mechanisms are determined by regression analysis (Eqn. (11)), and the results (Table 4) compare favorably to E_a values in the literature. For example, Gudbrandsson et al. (2011) report E_a between 24.2 kJ/mol (pH 11) and 54.1 kJ/mol (pH 3) for crystalline basalt. For glassy basalt, Gislason and Oelkers (2003) and report E_a to be 25.5 kJ/mol and independent of pH; whereas, Wolff-Boenisch et al. (2004a) report E_a to range between 27.2 kJ/mol (pH 4) and 41.3 kJ/mol (pH 10.6). The dissolution fluxes predicted by these equations are shown in Fig. 1. In the context of high P_{CO2} systems, e.g., geologic

Table 4
Results of multiple regression models for the silica release rate equation $\log J_{Si} = a + b/T + c\text{pH}$. The numbers in parentheses are one standard error for the fitted parameter.

	a	A	$\log k_{25^\circ}$	b	E_a	$c = n_H\,(-n_{OH})$	# data	R^2
glassy basalt								
pH < 6	2.699 (1.556)	5.00×10^{2}	−4.27	−2072 (430)	39.7	−1.013 (0.075)	67	0.742
pH > 6	−4.279 (0.839)	5.26×10^{-5}	−11.00	−2005 (288)	38.4	0.258 (0.036)	66	0.522
crystalline basalt								
pH < 6	0.869 (1.019)	7.40	−6.15	−2092 (272)	40.1	−0.680 (0.063)	13	0.931
pH > 6	−6.062 (0.978)	8.67×10^{-7}	−11.83	−1719 (304)	32.9	0.286 (0.057)	13	0.821

Table 5
Rate parameters for batch reactor simulations.

Mineral	Vol %	A m^2/m^3	Neutral mechanism		Acid mechanism			Base mechanism		
			k_{25} mol m^2 s^{-1}	E_a kJ mol^{-1}	k_{25} mol m^2 s^{-1}	E_a kJ mol^{-1}	n (H+)	k_{25} mol m^2 s^{-1}	E_a kJ mol^{-1}	n (H+)
Glassy basalt	100	6000	–	–	5.370×10^{-5}	39.7	1.013	1.000×10^{-11}	38.4	−0.258
Crystalline basalt	100	6000	–	–	7.080×10^{-7}	40.1	0.680	1.480×10^{-12}	32.9	−0.286
Composite basalt										
Forsterite[a]	15.8	948	2.291×10^{-11}	79.0	1.400×10^{-7}	67.2	0.470	–	–	–
Pyroxene[a]	34.0	2040	1.072×10^{-12}	78.0	1.500×10^{-7}	78.0	0.700	–	–	–
Plagioclase[a]	41.3	2478	1.230×10^{-11}	45.2	1.350×10^{-8}	42.1	0.626	–	–	–

[a] Rate model from Palandri and Kharaka (2004).

Table 6
Initial concentrations of primary aqueous species for the reactor models.

Primary aqueous species	Initial concentration (molal)
H^+	1.5×10^{-4} (pH 3.81)
H_4SiO_4	1.0×10^{-10}
O_2 (aq)	1.0×10^{-10}
HCO_3^-	1.5×10^{-4}
Al^{+3}	1.0×10^{-10}
Mg^{+2}	1.0×10^{-10}
Ca^{+2}	1.0×10^{-10}
Fe^{+2}	1.0×10^{-10}
Na^+	1.0×10^{-10}
K^+	1.0×10^{-10}

carbon sequestration, these models couple glassy and crystalline basalt dissolution to hydrogen ion production by mineral precipitation (e.g., $Ca^{2+} + HCO_3^- = CaCO_3 + H^+$). Fig. 2 compares the dissolution fluxes at 25 °C for glassy and crystalline basalt with the flux for the composite basalt, which is based on the weighted sum of the individual mineral rates. Fig. 2 shows that for pH < 6 the overall dissolution flux for the composite basalt is more than ten times slower than the flux for crystalline basalt predicted using the equation developed in this paper. Furthermore, for pH > 6 the rates predicted by the composite model are hundreds of times slower than the rate predicted for crystalline basalt.

3.2. TOUGHREACT simulations

Fig. 3 shows the evolution of solution and solid phase compositions for the batch reactor simulations. The initial pH is 3.8 due to the dissociation of the dissolved carbon dioxide (carbonic acid) to produce hydrogen ions and bicarbonate. During the early stage of the model reaction the pH is low and the hydrogen ions react rapidly with the basalt releasing Si, Ca, Mg, Na, Al, and Fe into solution. Soon the solution becomes saturated with respect to the alteration products and they begin to precipitate. Basalt dissolution and concurrent mineral precipitation continues until the carbonic acid is completely consumed. During this time the pH rises slowly as the rate of hydrogen ion consumption by basalt dissolution outpaces the rate of hydrogen ion release by mineral precipitation. After the carbonic acid is fully depleted, the pH jumps and the

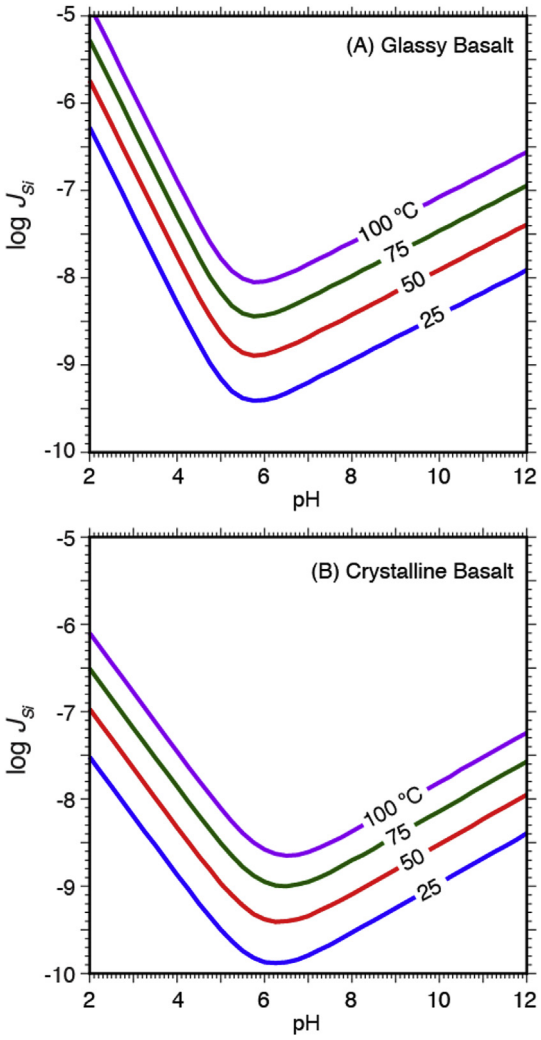

Fig. 1. Log J_{Si} versus pH for (A) glassy basalt and (B) crystalline basalt predicted by Equations 14 (A) and 15 (B) with parameters given in Table 4.

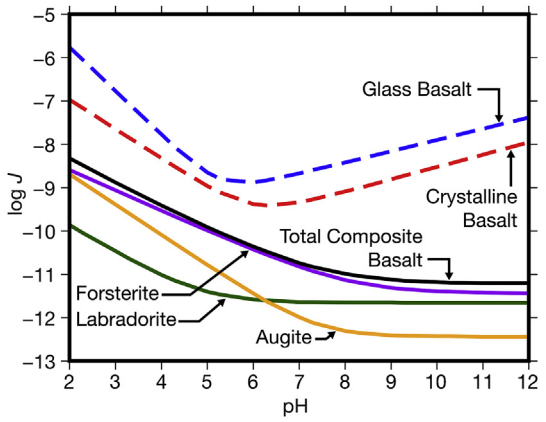

Fig. 2. Comparison of the dissolution fluxes (mol m^{-2} s^{-1}) at 25 °C for crystalline, glassy, and composite basalt models. The total composite basalt rate (black line) is the weighted sum of rates for forsterite (olivine), labradorite (plagioclase), and augite (pyroxene) computed using Equation (5) with parameters listed in Table 5. Forsterite, labradorite, and augite rates are from Palandri and Kharaka (2004).

cation concentrations drop as alteration products precipitate due to the pH increase. Beyond this time, the glassy and crystalline basalt models show no evidence of further reactions. By comparison, the concentrations in the composite basalt model continues to evolve in a complex way until the pH rises to near 12. Consistent with our expectations based on the relative rates, the pH jump occurs first in the glassy basalt simulation where the basalt dissolution rate is fastest and last in the composite basalt simulation where the dissolution rates are slowest. Additionally, the batch reactor models allowing for sodium bearing heulandite to precipitate exhibit near identical behavior with the exception that heulandite precipitation releases sufficient hydrogen ion to slightly lower pH in both the glassy and crystalline basalt reactors (see Supplementary Material, Fig. S5).

The semibatch reactor models reveal the intuitive findings that the glassy basalt fully dissolves first because its dissolution rate is fastest and the composite basalt is fully consumed last because its dissolution rate is slowest. Fig. 4 shows the temporal evolution of solid phase compositions and solution concentrations for the semibatch reactor simulations. As in the batch reactor models, the initial pH is 3.8 due to the presence of the dissolved carbon dioxide (carbonic acid), which dissociates to produce hydrogen and bicarbonate ions. In these simulations, the carbonic acid concentration is fixed by equilibrium with a P_{CO2} of 0.2 MPa (2 bar) for the duration of the simulation. This results in continuous supply of hydrogen ions due to continued carbonic acid dissociation. Fig. 4 shows that basalt dissolution and mineral precipitation patterns are similar to those in the batch reactor simulations in early time. However, because of the continuing supply of hydrogen ions, dissolution continues until all of the basalt is converted into alteration products. As the basalt is consumed, the pH slowly rises until it reaches a final value slightly less than eight. As pH rises beyond 6, both glassy and crystalline basalt dissolution rates increase (Fig. 1), which facilitates continued carbonate and silicate mineral precipitation releasing additional hydrogen ion and thus further driving basalt dissolution. The pH predicted by the numerical model represents a balance between these two processes. For each model, the final pH is set by the sodium and bicarbonate solution that is in equilibrium with the alteration minerals and a vapor phase with $P_{CO2} = 0.2$ MPa. The divalent cation concentrations decline with increasing pH due to the formation of carbonate minerals. Although some bicarbonate ions are consumed by carbonate mineral precipitation, the bicarbonate ion concentration increases with time because (1) additional CO_2 dissolves to replace the bicarbonate lost to the carbonate minerals and (2) the additional bicarbonate is needed to charge balance sodium ions, which are not incorporated into alteration products. Within the second set of semi-batch reactors that allow for sodium-bearing heulandite to precipitate, the sodium ion and bicarbonate concentrations are substantially lower as heulandite consumes sodium ions (see Supplementary Material, Fig. S6). Additionally, heulandite production releases additional hydrogen ion into solution, which results in lower pH ~6 in all three semi-batch reactors.

4. Discussion and conclusions

4.1. Rate equations

The rate equations reported in this paper apply to a composition representative of Icelandic basalts containing ~48% SiO_2. Wolff-Boenisch et al. (2004a) showed that volcanic glass dissolution rates change by 0.02–0.03 log units for every 1% change in silica content. This suggests that changing the wt% silica by ±5% would only change the rates by ±0.15 log units, which is well within the uncertainty of the predicted rates. Thus, we expect that rates for other basalt compositions should be similar to those for the Icelandic basalt materials.

The rate equations reported here are intended to summarize the rate information in the most efficient way, *i.e.* maximizing the R^2 while using a minimum number of regression variables. Theoretical constraints (*i.e.* the Arrhenius equation) and previous experience (*i.e.* the known effect of pH on dissolution rates) guided our choices of possible equations, which were winnowed using trial and error to find an efficient form. Other equations could fit the data equally well or even better. This means that we did not formulate our equations using an established theoretical model. Although these equations provide a suitable interpolation between the experimental data, they should not be extrapolated beyond the range of those data ($2 < pH < 12$ and $0° < T < 100$ °C).

The glassy basalt dissolution rates from Gislason and Oelkers (2003), Oelkers and Gislason (2001) and Wolff-Boenisch et al. (2004a) provide an excellent example of the challenge of fitting and interpreting this kind of dissolution rate data. Oelkers et al. (1994) and Oelkers (2001) developed and carefully explained a plausible theory for how the activity of Al^{3+} might inhibit the dissolution rate of aluminosilicate minerals and glasses. They used the data in Oelkers and Gislason (2001), Gislason and Oelkers (2003), and Wolff-Boenisch et al. (2004b) to show that glassy basalt dissolution rates correlate with $\log(a^3_{H^+}/a_{Al^{3+}})$ as predicted by that theory. Table 7 shows three different fits based on the 53 glassy basalt dissolution rate data for pH < 6 from the three sources mentioned above. The first row of that table shows that the rates correlate reasonably well with $1/T$ and $\log(a^3_{H^+}/a_{Al^{3+}})$ as predicted by the Al inhibition theory ($R^2 = 0.658$, the model explains 65.8% of the variance in $\log J_{Si}$). Nevertheless replacing the $\log(a^3_{H^+}/a_{Al^{3+}})$ term in this equation with pH gives a better fit ($R^2 = 0.731$, the model explains 73.1% of the variance in $\log J_{Si}$). This fit is clearly more efficient because it explains 7% more of the variance in $\log J_{Si}$ but with one fewer regression variable. Furthermore, expressing the $\log(a^3_{H^+}/a_{Al^{3+}})$ variable from the first equation as in terms of pH and $\log a_{Al^{3+}}$ gives an even better fit ($R^2 = 0.770$, the model explains 77.0% of the variance in $\log J_{Si}$). However, this 3.9% improvement in the fit comes at the expense of using an additional regression variable. In our opinion, the additional predictive value of this more complicated equation does not offset the analytical and computational effort needed to determine the aluminum activities, so we chose to exclude the aluminum activity from our regression

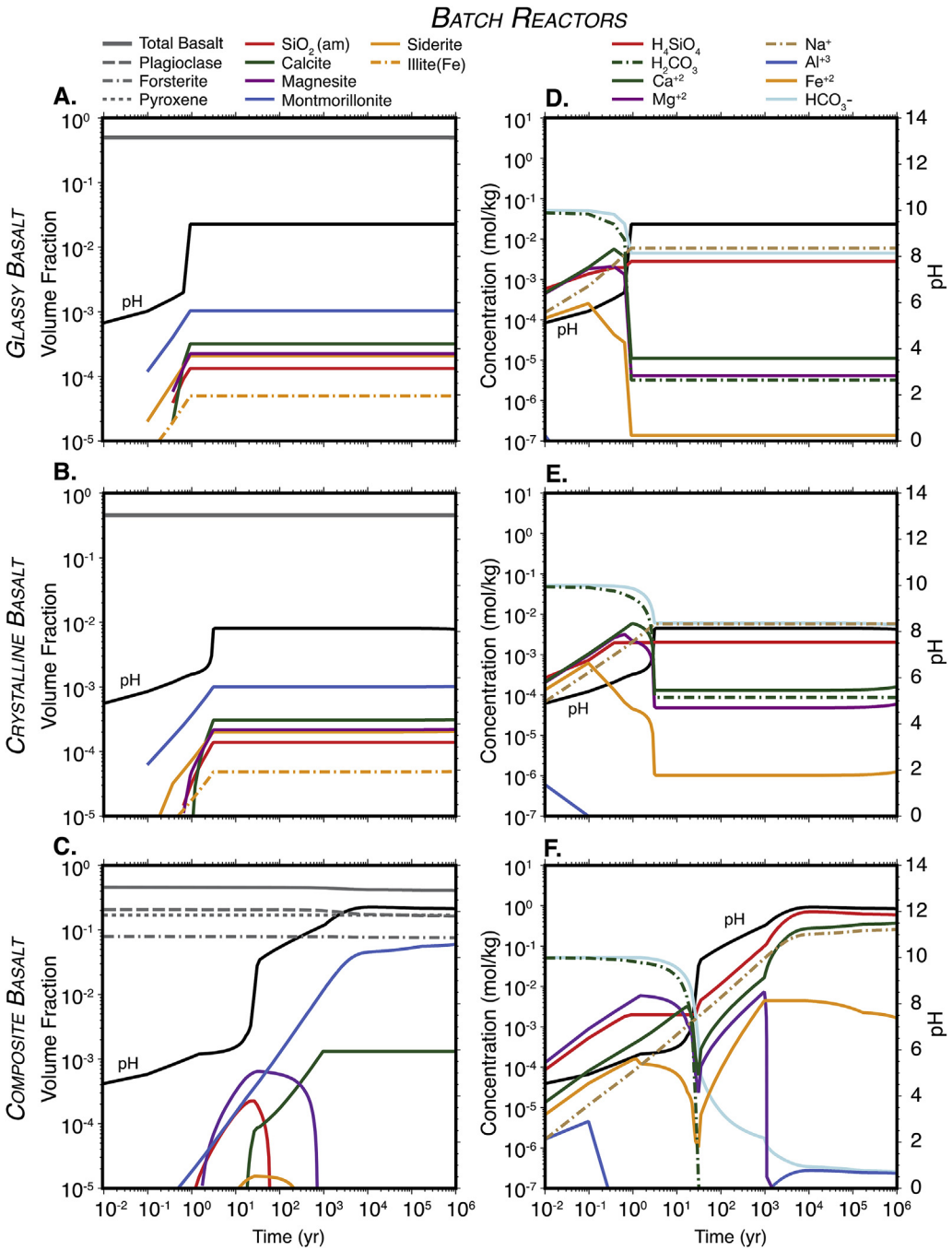

Fig. 3. Modeled compositions for batch reactors containing glassy (A, D), crystalline (B, E) and composite basalt (C, F) as a function of time (log scale). The volume fraction of solid phases is shown by the graphs on the left and the solution concentrations are shown by the graphs of the right. The solution pH is shown by the heavy black line on all graphs with corresponding scale on the right axis of each graph. Note that potassium concentration is below 10^{-7} mol/kg for all models.

models.

This is only one example of the difficulties associated with selecting and interpreting dissolution rate equations. Multiple rate equations can be fit to data sets because the regression variables in those equations are correlated with each other. Rimstidt (2015) showed that quartz dissolution rates were fit equally well by five different rate equations because of strong correlations among the regression variables. That means that even though a data set is well described by a rate equation, the chosen regression variables may not reflect species that actually participate in the activated complex for the rate-determining step. The different activation energy values reported in Table 7 are even more disconcerting. They arise because the calculated aluminum activity values were adjusted for the temperature variation of the hydrolysis constants. As a result, the enthalpy of those hydrolysis reactions was incorporated into the activation energy values reported in the first and third, but not in the second, equation. Rimstidt (2015) shows a simpler example for quartz dissolution in sodium bearing solutions where the activation energy calculated from an equation written in terms of hydrogen ion activity is 88.0 kJ/mol, but for an equation written in terms of hydroxide ion activity the activation energy is 71.6 kJ/mol. Variable activation energy values do not occur for rate equations

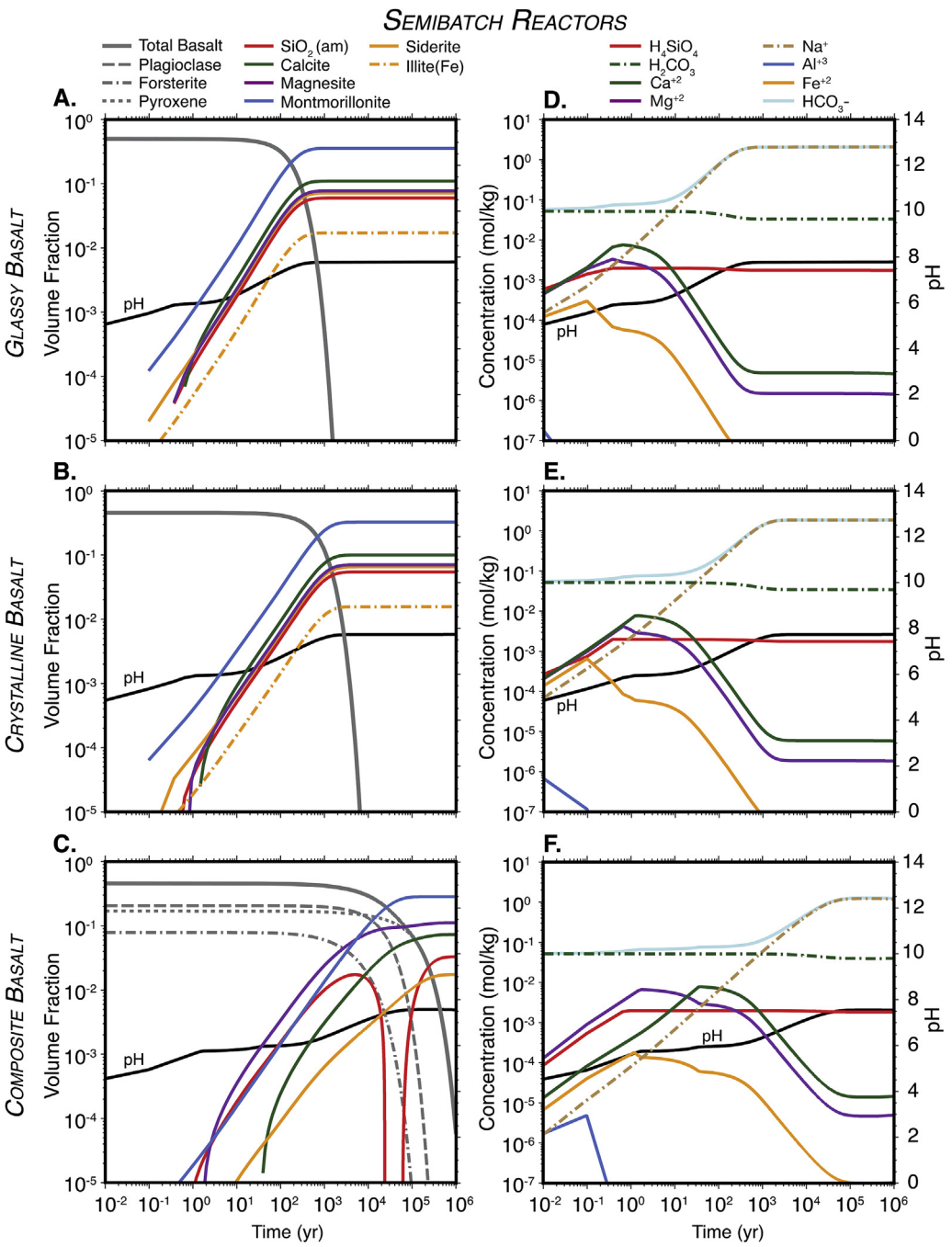

Fig. 4. Modeled compositions for semibatch reactors with fixed P_{CO2} of 0.2 MPa (2 bar) containing glassy (A, D), crystalline (B, E) and composite basalt (C, F) as a function of time (log scale). The volume fraction of solid phases is show by the graphs on the left and the solution concentrations are shown by the graphs of the right The solution pH is shown by the heavy black line on all graphs with corresponding scale on the right axis of each graph. Note that potassium concentration is below 10^{-7} mol/kg for all models.

Table 7
Results of fitting 53 rate data from Gislason and Oelkers (2003), Oelkers and Gislason (2001) and Wolff-Boenisch et al. (2004a) to three different rate equations.

Equation	R^2	E_a, kJ/mol
$\log J_{Si} = -1.04(1.72) - \frac{1334(511)}{T} + 0.438(0.046)\log\left(\frac{a_{H^+}^3}{a_{Al^{3+}}}\right)$	0.658	25.5
$\log J_{Si} = 6.64(1.76) - \frac{3259(489)}{T} - 0.985(0.086)pH$	0.731	62.4
$\log J_{Si} = 4.42(1.81) - \frac{2652(502)}{T} - 1.22(0.12)pH - 0.185(0.064)\log a_{Al^{3+}}$	0.770	50.8

Numbers in brackets are one standard error for the fitted parameter.

based on speciation at a reference temperature (e.g. quench pH), as is the case for the rate equations for amorphous silica dissolution in Rimstidt et al. (2016), but this means that the computed activation energy does not correctly account for the change in speciation with temperature. These examples should serve as a deterrent to anyone trying to infer or to test a reaction mechanism based solely on rate equations and/or activation energy values. In all but the very simplest cases this approach is likely to be misleading.

4.2. TOUGHREACT simulations

The batch reactor models show that dissolved CO_2 is quickly consumed by reaction with basalt materials, after which the reactions effectively cease (Fig. 3). This is consistent with the persistance of unaltered basalt materials for geological time spans. For example, Madrigal et al. (2016) report finding fresh pillow basalt glasses with ages in excess of 100 million years. This highlights the importance of CO_2 as a source of the hydrogen ions needed for rock alteration and weathering.

The glassy and crystalline basalt batch reactor models show a clear conclusion of reactions after the CO_2 is consumed and the pH reaches near eight (Fig. 3A and B). This is consistent with pH values that range between 7 and 9 in groundwaters produced from basalts (Flaathen et al., 2009). However, the composite basalt model reactions continue until the pH climbs to near 12 (Fig. 3C). This somewhat disconcerting result appears to be due to treating the basalt minerals as an aggregate physical mixture of ~1 mm diameter grains rather than a fine scale assemblage of dissolving oxide components. In the composite basalt model, significant plagioclase dissolution continues to consume hydrogen ions and release sodium and calcium ions after the dissolved CO_2 is consumed (Fig. 3F). The rising pH causes the conversion of bicarbonate into carbonate, which drives calcite precipitation and keeps the plagioclase undersaturated. This continues until all of the bicarbonate has been converted to carbonate. This high pH is not predicted by the glassy or crystalline basalt models because they do not consider plagioclase as a discrete phase. As a result, the crystalline basalt dissolution rate equation presented here may be preferable to modeling basalt reactivity as a composite assemblage of individual mineral dissolution rates.

In the semibatch reactor simulations, the fixed P_{CO2} provides a constant supply of carbonic acid, which results in a constant supply of hydrogen ions that are needed for basalt dissolution. Fig. 4 shows that there is remarkable agreement in both the alteration products and concentrations of aqueous species over time among glassy, crystalline and composite basalt models. Based on the selection of alteration products, all three models predict that the Si and Al from the basalt will mostly end up as montmorillonite and that calcite and magnesite will be the most abundant host minerals for carbonate (Fig. 4A–C). In addition, they predict that the long term solution pH will be near 8 and the predominant solution species will be Na^+ and HCO_3^- (Fig. 4D–F). This is consistent with water chemistries found in the Main Ethiopian Rift Valley (Africa) where reactions of groundwaters affected by high rates of CO_2 outgassing are near neutral to slightly alkaline sodium bicarbonate solutions (Gizaw, 1996).

The main differences among the semibatch reactor simulations arises from the differences in the dissolution rates. The rapidly dissolving glassy basalt is completely altered first, followed by the crystalline basalt and then slowest dissolving composite basalt. Between pH 5 and 7, the dissolution rate of crystalline basalt is 1–2 log units faster than the total composite rate (Fig. 2). Moreover, for pH > 6, the crystalline basalt rate increases in accordance with the base rate mechanism; whereas, the composite rate continues decreasing as the acid mechanism becomes weaker and the total rate reverts to the weighted sum of the neutral dissolution rates for each component mineral (Fig. 2). The other notable difference between the crystalline and composite basalt reactor models results from the step-wise mineral dissolution in the composite basalt reactor (Fig. 4C, gray dashed lines). Although the general reaction progress is remarkably similar between the reactors, the stepwise dissolution of the minerals is notable for the composite basalt in the last stages of basalt consumption. The model shows that forsterite is almost completely consumed before plagioclase and pyroxene show appreciable dissolution (Fig. 4C). This occurs because the dissolution rate of forsterite is ~1–2 log units faster than plagioclase (labradorite) and pyroxene (augite) over the pH range of 5–7 (Fig. 2). As a result, magnesite formed from Mg released by the dissolving olivine is the dominant alteration product through the first 1,000 years of simulation. Nevertheless, the much larger volume fractions of plagioclase and pyroxene in comparison to forsterite results in sufficient Ca and Fe concentrations for some calcite and siderite to precipitate. Beyond 1,000 years, the pH increases above 7 and the pyroxene dissolution rate decreases substantially (Fig. 2). This causes reactions in the composite basalt model to be governed primarily by plagioclase dissolution through ~12,000 years, after which time the plagioclase volume fraction becomes small enough to permit pyroxene dissolution.

The somewhat troubling step-wise dissolution pattern exhibited by the composite basalt model occurs because the solution in the simulation has access to all of the minerals all of the time. However, in real rocks the solution can only access minerals adjacent to the pore space or fracture surface within the rock. In this case, the rock face becomes depleted in the fastest dissolving phase(s) and enriched in the slowest dissolving phase(s). In order for our model to reflect this constraint we would need to adjust the relative surface areas of the mineral phases to diminish the olivine surface area until its dissolution rate matches the slower dissolution rates of plagioclase and pyroxene. Although the TOUGHREACT simulator implements dynamically changing surface area resulting from dissolution (Apx. G in Xu et al., 2014), the effect is muted in the composite basalt reactor due to the orders-of-magnitude difference in dissolution rates for forsterite, pyroxoene (augite), and plagioclase (labradorite). Moreover, the method for surface area calculation in TOUGHREACT assumes all surface area is in contact with the solution, and does not account for masking effects due to slower dissolving minerals. In contrast, the dissolution behavior of the crystalline basalt model developed in this study implicitly accounts for this problem by dissolving the aggregate assemblage pursuant to the silica release rates described by Gudbrandsson et al. (2011). However, the crystalline basalt rate model does not decouple the dissolution rates of each component mineral, which may be desirable in some circumstances. Nevertheless, the crystalline basalt model presented here seems well suited for early time behavior at high P_{CO2} (e.g., CCS models in basalt) because the rate equation implicitly accounts for the simultaneous dissolution of olivine, plagioclase, and pyroxene, which is expected when a CO_2-rich fluid enters a basalt fracture network.

Ultimately, it is up to the modeler to decide which approach most reasonably approximates the system under investigation, and in this study we report a simplified method for modeling crystalline and glassy basalt dissolution. The crystalline dissolution model compares favorably with a more traditional (and complex) approach comprising individual mineral species, and in some circumstances may yield a more reasonable representation of the system. In order to facilitate implementation of these rate equations, Supplemental Information (Tables S1–S2) with this paper includes the thermodynamic database entries for crystalline and glassy basalt, as well as the kinetic rate equation entries for the chemical. inp file used in TOUGHREACT v3.2-OMP (Xu et al., 2014).

Acknowledgements

Pollyea dedicates this manuscript to his friend and mentor, Professor Jerry P. Fairley, who taught him the danger of Maslow's Hammer. The authors gratefully acknowledge the insightful review comments provided by Dr. Domenik Wolff-Boenisch, the result of which have tremendously improved the quality of this manuscript. This study was funded in part by the U.S. Department of Energy National Energy Technology Laboratory through cooperative agreement DE-FE0023381 (PI Pollyea).

Appendix A. Supplementary data

Supplementary data related to this article can be found at http://dx.doi.org/10.1016/j.apgeochem.2017.03.020.

References

Aradóttir, E.S.P., Sonnenthal, E.L., Björnsson, G., Jonsson, H., 2012a. Multidimensional reactive transport modeling of CO_2 mineral sequestration in basalts at the Hellisheidi geothermal field, Iceland. Int. J. Greenh. Gas Control 9, 24–40.

Aradóttir, E.S.P., Sonnenthal, E.L., Jónsson, H., 2012b. Development and evaluation of a thermodynamic dataset for phases of interest in CO_2 mineral sequestration in basaltic rocks. Chem. Geol. 304, 26–38.

Bacon, D.H., Ramanathan, R., Schaef, H.T., McGrail, B.P., 2014. Simulating geologic co-sequestration of carbon dioxide and hydrogen sulfide in a basalt formation. Int. J. Greenh. Gas Control 21, 165–176.

Blanc, P., Lassin, A., Piantone, P., Azaroual, M., Jacquemet, N., Fabbri, A., Gaucher, E.C., 2012. Thermoddem: a geochemical database focused on low temperature water/rock interactions and waste materials. Appl. Geochem. 27 (10), 2107–2116.

Flaathen, T.K., Gislason, S.R., Oelkers, E.H., Sveinbjornsdottir, A.E., 2009. Chemical evolution of the Mt. Hekla, Iceland, groundwaters: a natural analogue for CO_2 sequestration in basaltic rocks. Appl. Geochem. 24, 463–474.

Flaathen, T.K., Gislason, S.R., Oelkers, E.H., 2010. The effect of aqueous sulphate on basaltic glass dissolution rates. Chem. Geol. 277, 345–354.

Gislason, S.R., Wolff-Boenisch, D., Stefánsson, A., Oelkers, E.H., Gunnlaugsson, E., Sigurdardottir, H., Sigfusson, B., Broecker, W.S., Matter, J.M., Stute, M., Axelsson, G., 2010. Mineral sequestration of carbon dioxide in basalt: a pre-injection overview of the CarbFix project. Int. J. Greenh. Gas Control 4 (3), 537–545.

Gislason, S.R., Oelkers, E.H., 2003. Mechanism, rates, and consequences of basaltic glass dissolution: II. An experimental study of the dissolution rates of basaltic glass as a function of pH and temperature. Geochim. Cosmochim. Acta 67, 3817–3832.

Gizaw, B., 1996. The origin of high bicarbonate and fluoride concentrations in waters of the Main Ethiopian Rift Valley, East African Rift system. J. Afr. Earth Sci. 22 (4), 391–402.

Goldberg, D.S., Kent, D.V., Olsen, P.E., 2010. Potential on-shore and off-shore reservoirs for CO_2 sequestration in Central Atlantic magmatic province basalts. Proc. Natl. Acad. Sci. 107 (4), 1327–1332.

Goldberg, D.S., Takahashi, T., Slagle, A.L., 2008. Carbon dioxide sequestration in deep-sea basalt. Proc. Natl. Acad. Sci. 105 (29), 9920–9925.

Gudbrandsson, S., Wolff-Boenisch, D., Gislason, S., Oelkers, E.H., 2011. An experimental study of crystalline basalt dissolution from $2 \leq pH \leq 11$ and temperatures from 5 to 75°C. Geochim. Cosmochim. Acta 75, 5496–5509.

Gysi, A.P., Stefánsson, A., 2012. CO_2–water–basalt interaction. Low temperature experiments and implications for CO_2 sequestration into basalts. Geochim. Cosmochim. Acta 81, 129–152.

Gysi, A.P., Stefánsson, A., 2011. CO_2–water–basalt interaction. Numerical simulation of low temperature CO_2 sequestration into basalts. Geochim. Cosmochim. Acta 75 (17), 4728–4751.

Jayaraman, K.S., 2007. India's carbon dioxide trap. Nature 445 (7126), 350–350.

Madrigal, P., Gazel, E., Flores, K.E., Bizimis, M., Jicha, B., 2016. Record of massive upwellings from the Pacific large low shear velocity province. Nat. Commun. 7, 13309.

Matter, J.M., Stute, M., Snæbjörnsdottir, S.Ó., Oelkers, E.H., Gislason, S.R., Aradóttir, E.S., Sigfusson, B., Gunnarsson, I., Sigurdardottir, H., Gunnlaugsson, E., Axelsson, G., Alfredsson, H.A., Wolff-Boenisch, D., Mesfin, K., Fernandez de la Reguera Taya, D., Hall, J., Dideriksen, K., Broecker, W.S., 2016. Rapid carbon mineralization for permanent disposal of anthropogenic carbon dioxide emissions. Science 352 (6291), 1312–1314.

Matter, J.M., Kelemen, P.B., 2009. Permanent storage of carbon dioxide in geological reservoirs by mineral carbonation. Nat. Geosci. 2 (12), 837–841.

McGrail, B.P., Schaef, H.T., Spane, F.A., Cliff, J.B., Qafoku, O., Horner, J.A., Thompson, C.J., Owen, A.T., Sullivan, C.E., 2017. Field validation of supercritical CO2 reactivity with basalts. Environ. Sci. Technol. Lett. 4, 6–10.

McGrail, B.P., Spane, F.A., Amonette, J.E., Thompson, C.R., Brown, C.F., 2014. Injection and monitoring at the wallula basalt pilot project. Energy Procedia 63, 2939–2948.

McGrail, B.P., Schaef, H.T., Ho, A.M., Chien, Y.J., Dooley, J.J., Davidson, C.L., 2006. Potential for carbon dioxide sequestration in flood basalts. J. Geophys. Res. Solid Earth 111 (B12).

Moya-Laraño, J., Corcobado, G., 2008. Plotting partial correlation and regression in ecological studies. Web Ecol. 8, 35–46.

Oelkers, E.H., 2001. General kinetic description of multioxide silicate mineral and glass dissolution. Geochim. Cosmochim. Acta 65, 3703–3719.

Oelkers, E.H., Schott, J., Devidal, J.-L., 1994. The effect of aluminum, pH, and chemical affinity of the rates of aluminosilicate dissolution reactions. Geochim. Cosmochim. Acta 58, 2011–2024.

Oelkers, E.H., Gislason, S.R., 2001. The mechanism, rates and consequences of basaltic glass dissolution: I. An experimental study of the dissolution rates of basaltic glass as a function of aqueous Al, Si and oxalic acid concentration at 25°C and pH = 3 and 11. Geochim. Cosmochim. Acta 65, 3671–3681.

Palandri, J.L., Kharaka, Y.K., 2004. A compilation of rate parameters of water-mineral interaction kinetics for application to geochemical modeling. U.S. Geological Survey, Menlo Park, California, p. 64.

Paul, A., 1977. Chemical durability of glasses; a thermodynamic approach. J. Mater. Sci. 12 (11), 2246–2268.

Pollyea, R.M., Fairley, J.P., Podgorney, R.K., Mcling, T.L., 2014. Physical constraints on geologic CO_2 sequestration in low-volume basalt formations. Geol. Soc. Am. Bull. 126 (3–4), 344–351.

Pollyea, R.M., Fairley, J.P., 2012. Implications of spatial reservoir uncertainty for CO_2 sequestration in the east Snake River Plain, Idaho (USA). Hydrogeol. J. 20 (4), 689–699.

Rimstidt, J.D., 2015. Rate equations for sodium catalyzed quartz dissolution. Geochim. Cosmochim. Acta 167, 195–204.

Rimstidt, J.D., Zhang, Y., Zhu, C., 2016. Rate equations for sodium catalyzed amorphous silica dissolution. Geochim. Cosmochim. Acta 195, 120–125.

Schaef, H.T., McGrail, B.P., Owen, A.T., Arey, B.W., 2013. Mineralization of basalts in the CO_2–H_2O–H_2S system. Int. J. Greenh. Gas Control 16, 187–196.

Sigfusson, B., Gislason, S.R., Matter, J.M., Stute, M., Gunnlaugsson, E., Gunnarsson, I., Aradóttir, E.S., Sigurdardottir, H., Mesfin, K., Alfredsson, H.A., Wolff-Boenisch, D., 2015. Solving the carbon-dioxide buoyancy challenge: the design and field testing of a dissolved CO_2 injection system. Int. J. Greenh. Gas Control 37, 213–219.

Stefánsson, A., 2001. Dissolution of primary minerals of basalt in natural waters: I. Calculation of mineral solubilities from 0 C to 350 C. Chem. Geol. 172 (3), 225–250.

Techer, I., Advocat, T., Lancelot, J., Liotard, J.M., 2001. Dissolution kinetics of basaltic glasses: control by solution chemistry and protective effect of the alteration film. Chem. Geol. 176 (1), 235–263.

Velleman, P.F., Welsch, R.E., 1981. Efficient computing of regression diagnostics. Am. Stat. 35, 234–242.

Wolff-Boenisch, D., Gislason, S.R., Oelkers, E.H., Putnis, C.V., 2004a. The dissolution rates of natural glasses as a function of their composition at pH 4 and 10.6, and temperatures from 25 to 74°C. Geochim. Cosmochim. Acta 68, 4843–4858.

Wolff-Boenisch, D., Gislason, S.R., Oelkers, E.H., 2004b. The effect of fluoride on the dissolution rates of natural glasses at pH 4 and 25 C. Geochim. Cosmochim. Acta 68 (22), 4571–4582.

Xu, T., Sonnenthal, E., Spycher, N., Zheng, L., 2014. TOUGHREACT V3.0-OMP Reference Manual: a Parallel Simulation Program for Non-isothermal Multiphase Geochemical Reactive Transport. LBNL-DRAFT. Earth Sciences Division, Lawrence Berkeley National Laboratory. University of California, Berkeley, CA, p. 94720 (June).

Supplemental Information
Rate equations for modeling carbon dioxide sequestration in basalt

Ryan M. Pollyea & J. Donald Rimstidt
Virginia Polytechnic Institute & State University

Table S1: TOUGHREACT thermodynamic database entries for glassy and crystalline basalt – compatible with ThermodemmV1.10

```
'basalt_glass'                    120.919   38.488   9   -2.630  'H+'  -0.685  'H2O'  1.000  'H4SiO4'  0.358  'Al+3'  0.190  'Fe+2'
0.281  'Mg+2'  0.264  'Ca+2'  0.079 'Na+'  0.008  'K+'
'basalt_glass'                      10.5805   9.3367  7.9099  6.6082  5.3187  4.2778  3.3953  2.6068
'basalt_glass'
# Pollyea & Rimstidt (2017, in review) - based on weighted combination of component oxide constants per Equation 13 in manuscript.

'basalt_xtal'                     120.919   38.488   9   -2.630  'H+'  -0.685  'H2O'  1.000  'H4SiO4'  0.358  'Al+3'  0.190  'Fe+2'
0.281  'Mg+2'  0.264  'Ca+2'  0.079 'Na+'  0.008  'K+'
'basalt_xtal'                        9.5805   8.3367  6.9099  5.6082  4.3187  3.2778  2.3953  1.6068
'basalt_xtal'
# Pollyea & Rimstidt (2017, in review) - lower glass constants by one order of magnitude.
```

Table S2: TOUGHREACT input entries (`chemical.inp`) to implement kinetic dissolution rates for glassy and crystalline basalt

```
'basalt_glass'          1          1     0     0                              ! BASALT GLASS - Pollyea & Rimstidt (2017)
                        0.000E-00  2     1.0   1.0   0.0  0.0   0.0   0.0   ! Acid & base dissolution mechanisms
                        2                                                    !  - no neutral mechanism
                        5.370E-05  39.7  1     H+'   1.013                   !  - acid mechanism
                        1.000E-11  38.4  1    'H+'  -0.258                   !  - base mechanism

'basalt_xtal'           1          1     0     0                              ! BASALT XTAL - Pollyea & Rimstidt (2017)
                        0.000E-00  2     1.0   1.0   0.0  0.0   0.0   0.0   ! Acid & base dissolution mechanisms
                        2                                                    !  - no neutral mechanism
                        7.080E-07  40.1  1    'H+'   0.680                   !  - acid mechanism
                        1.480E-12  32.9  1    'H+'  -0.286                   !  - base mechanism
```

Supplemental Information
Rate equations for modeling carbon dioxide sequestration in basalt
Ryan M. Pollyea & J. Donald Rimstidt
Virginia Polytechnic Institute & State University

Data used to create rate equations

Table S3: Data used for glassy basalt dissolution equation.

Experiment	T, °C	pH	log J(geo)
Gislason and Oelkers (2003)			
BG5-2	6.00	4.37	-9.08
BG5-5	6.00	4.85	-9.33
BG5-10	7.00	6.57	-9.48
BG5-13	7.00	7.74	-9.39
BG5-17	7.00	8.97	-8.97
BG5-20	7.00	9.79	-9.04
BG5-22	7.00	10.58	-8.88
BG5-27	10.00	3.34	-7.54
BG5-28	11.00	2.25	-6.87
BG2-11	30.00	4.17	-8.36
BG-21	30.00	3.31	-7.14
BG2-40	30.00	2.40	-6.09
BG3-8	29.00	7.00	-8.44
BG3-11	30.00	8.19	-8.17
BG3-20	30.00	9.13	-7.85
BG3-23b	30.00	10.20	-7.82
BG3-27	30.00	10.80	-7.64
BG6-2	50.00	3.94	-7.77
BG6-10	50.00	7.03	-8.14
BG6-15	50.00	7.79	-7.71
BG6-18	50.00	8.93	-7.73
BG6-23	50.00	9.79	-7.68
BG6-26	50.00	10.33	-7.36
BG6-37	50.00	3.10	-6.53
BG6-39	49.00	2.14	-5.88
BG4-2	30.00	5.35	-8.59
BG4-6	60.00	5.23	-7.71
BG4-9	100.00	5.91	-7.20
BG4-15	149.00	7.12	-6.55
Oelkers and Gislason (2001)			
Bg98–6–18	25.00	3.05	-7.20
Bg98–6–25	25.00	3.08	-6.94
Bg98–6–31	25.00	3.01	-7.70

Ryan M. Pollyea & J. Donald Rimstidt
Virginia Polytechnic Institute & State University

Experiment	T, °C	pH	log J(geo)
Bg98–8–3	25.00	3.00	-6.90
Bg98–8–14	25.00	3.04	-7.09
Bg98–8–20	25.00	3.03	-6.94
Bg98–1–6	25.00	3.09	-6.89
Bg98–1–19	25.00	3.08	-6.81
Bg98–7–05	25.00	3.08	-6.97
Bg98–7–34	25.00	3.03	-6.95
Bg98–7–55	25.00	3.00	-6.94
Bg99–2–03	25.00	2.99	-7.19
Bg99–2–05	25.00	2.96	-7.73
Bg99–2–08	25.00	3.11	-7.78
Bg99–2–11	25.00	3.03	-7.66
Bg99–2–12	25.00	3.00	-7.39
Bg99–2–13	25.00	2.98	-7.10
Bg99–2–15	25.00	3.11	-7.32
Bg99–2–17	25.00	3.04	-7.37
Bg99–3–02	25.00	3.05	-7.05
Bg99–3–04	25.00	3.03	-7.03
Bg99–3–05	25.00	2.98	-7.22
Bg99–3–09	25.00	3.00	-7.27
Bg99–3–11	25.00	2.95	-7.45
Bg99–3–13	25.00	2.97	-7.50
Bg99–3–14	25.00	3.08	-7.17
Bg99–3–15	25.00	2.98	-7.02
Bg99–3–16	25.00	3.04	-7.30
Bg99–3–17	25.00	3.00	-7.28
Bg99–4–2	25.00	3.10	-7.20
Bg99–4–4	25.00	2.91	-6.79
Bg99–4–10	25.00	3.03	-6.91
BG5–8	25.00	10.97	-8.03
BG5–15	25.00	10.97	-8.15
BG5–18	25.00	10.96	-8.29
BG7–5	25.00	10.98	-8.08
BG7–8	25.00	10.98	-8.57
BG7–12	25.00	11.00	-8.19
BG7–16	25.00	10.92	-8.66
BG7–22	25.00	10.97	-8.23

Experiment	T, °C	pH	log J(geo)
BG8–13	25.00	11.00	-8.22
BG8–25	25.00	10.99	-8.24
BG8–26	25.00	11.00	-8.30
BG8–31	25.00	11.02	-8.32
BG8–34	25.00	11.00	-8.26
BG8–35	25.00	10.94	-8.76
BG9–14	25.00	11.06	-8.34
BG9–19	25.00	11.01	-8.96
BG9–21	25.00	10.99	-8.86
BG9–25	25.00	11.04	-8.32
Flaathen et al. (2010)			
13-A	50.00	3.00	-7.27
1-A	50.00	2.92	-7.10
10-A	50.00	3.08	-7.13
2-A	50.00	3.05	-7.14
12-B	50.00		-7.04
14-B	50.00	4.23	-8.50
14-A	50.00		-8.60
3-A	50.00	4.05	-8.30
4-A	50.00	4.05	-8.32
5-A	50.00	3.95	-8.11
6-A	50.00	5.01	-9.47
11-P	50.00	5.06	-9.25
9-A	50.00	5.13	-9.24
7-A	50.00	5.02	-9.14
8-A	50.00	5.06	-8.87
11-T	50.00	5.84	-9.46
11-S	50.00	6.06	-9.28
11-Q	50.00	6.01	-9.27
11-R	50.00	5.97	-9.25
11-J	50.00	8.01	-8.92
11-F	50.00	7.99	-8.76
11-O	50.00	8.10	-8.82
11-G	50.00	8.04	-8.84
11-H	50.00	8.02	-8.90
11-I	50.00	7.99	-8.87
11-K	50.00	7.97	-8.91

Ryan M. Pollyea & J. Donald Rimstidt
Virginia Polytechnic Institute & State University

Experiment	T, °C	pH	log J(geo)
12-A	50.00	9.02	-8.22
12-D	50.00	9.00	-8.39
11-L	50.00	9.05	-8.47
11-M	50.00	9.08	-8.53
12-B	50.00	9.03	-8.44
12-C	50.00	8.98	-8.43
11-A	50.00	10.02	-7.77
11-N	50.00	9.98	-7.86
11-B	50.00	10.08	-7.80
11-C	50.00	10.07	-7.89
11-E	50.00	10.05	-7.95
11-D	50.00	10.06	-7.92
Wolff-Boenisch et al. (2004)			
SS-5	25.00	4.17	-8.95
SSF-4	25.00	4.17	-8.82
SS(2)-8	25.00	10.65	-7.86
SS(3)-4	25.00	10.49	-7.84
ELD-20	25.00	4.00	-8.90
ELD(3)-5	25.00	10.77	-7.81
KAT-6	25.00	4.17	-8.80
KAT(2)-4	25.00	10.50	-7.64
KRA-6	25.00	4.12	-9.02
KRA-9	32.00	4.06	-8.99
KRA-17	40.00	4.08	-8.82
KRA(2)-4	25.00	10.78	-8.23
KRA(2)-8	39.00	10.29	-7.92
KRA(2)-11	54.00	9.85	-7.67
GR-6	25.00	4.07	-9.19
GR(1)-4	25.00	10.61	-7.71
GR(2)-5	25.00	10.67	-7.79
GR(3)-4	25.00	10.63	-7.99

Table S4: Data for crystalline basalt dissolution equation.

Experiment	T, °C	pH	log J(geo)
Gudbrandsson et al. (2011)			
02-05	5.00	2.04	-7.98
03-05	5.00	3.05	-8.66
03-25	25.00	2.94	-8.31
03-50	50.00	3.16	-7.30
04-05	5.00	4.06	-9.56
04-25	25.00	4.13	-8.85
04-50	50.00	4.09	-8.57
04-75	75.00	4.04	-8.21
05-05	5.00	5.00	-10.04
05-25	25.00	5.03	-9.67
05-50	50.00	5.14	-9.30
05-75	75.00	5.65	-8.70
06-25	25.00	5.86	-9.99
07-50	50.00	6.89	-9.49
07-75	75.00	6.59	-8.67
09-05	5.00	9.24	-9.80
09-25	25.00	9.22	-9.48
09-50	50.00	9.28	-9.02
09-75	75.00	9.27	-8.60
10-25	25.00	10.10	-8.93
10-50	50.00	10.12	-8.29
10-75	75.00	10.09	-8.07
11-05	5.00	10.74	-8.78
11-25	25.00	11.01	-8.49
11-50	50.00	10.76	-8.43
11-75	75.00	10.96	-7.81

Ryan M. Pollyea & J. Donald Rimstidt
Virginia Polytechnic Institute & State University

Table S5: Concentrations of all aqueous species at initial time for the models.

Primary Aqueous Species	Initial Concentration (molal)	Aqueous Complexes	Initial Concentration (molal)
H^+	1.5×10^{-4} (pH 3.81)	$CO_2(aq)^\dagger$	5.2×10^{-2}
H_4SiO_4	1.0×10^{-10}	CO_3^{-2}	5.0×10^{-11}
$O_2(aq)$	1.0×10^{-10}	OH^-	6.7×10^{-11}
HCO_3^-	1.5×10^{-4}	$Al(OH)_2^+$	6.4×10^{-12}
Al^{+3}	1.0×10^{-10}	$Al(OH)_3^0$	8.9×10^{-16}
Mg^{+2}	1.0×10^{-10}	$Al(OH)_4^-$	2.1×10^{-18}
Ca^{+2}	1.0×10^{-10}	$FeOH^+$	2.0×10^{-16}
Fe^{+2}	1.0×10^{-10}	$MgOH^+$	1.3×10^{-18}
Na^+	1.0×10^{-10}	$CaOH^+$	1.0×10^{-19}
K^+	1.0×10^{-10}	$H_3SiO_4^-$	1.0×10^{-16}

In TOUGHREACT, all aqueous complexes (secondary aqueous species) are formulated as combinations of primary aqueous species. In particular, $CO_2(aq) = HCO_3^- + H^+$. As a result, the total HCO_3^- reported for the initial condition in the simulation code is 5.2019×10^{-2} molal; however, there is 5.1865×10^{-2} molal $CO_2(aq)$, which leaves 1.54×10^{-4} molal HCO_3^- available in solution. Put differently, the concentration of available HCO_3^- is the difference between total HCO_3^- and $CO_2(aq)$ for the model scenarios presented here.

Supplemental Information
Rate equations for modeling carbon dioxide sequestration in basalt
Ryan M. Pollyea & J. Donald Rimstidt
Virginia Polytechnic Institute & State University

JMP output

Figure S1: JMP output for glassy basalt rates pH < 6.

Source
- Flaathen et al. 2010
- Gislason & Oelkers 2003
- Oelkers & Gislason 2001
- Wolff-Boenisch et al. 2004

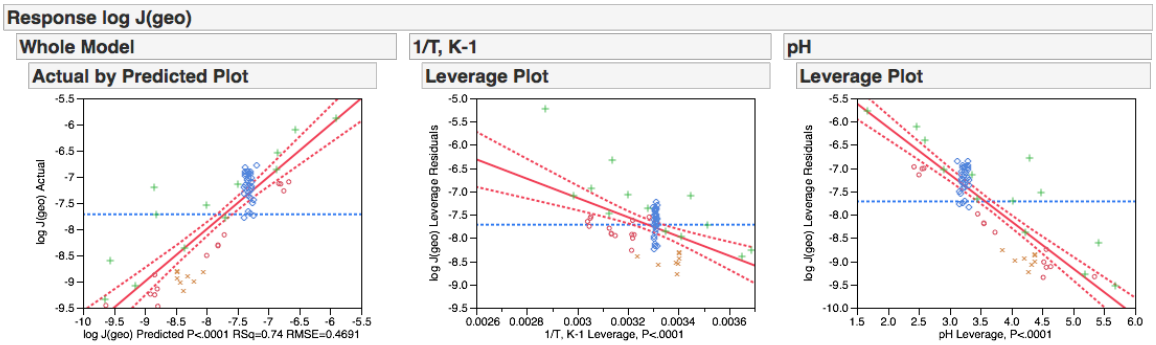

Summary of Fit

RSquare	0.741795
RSquare Adj	0.733726
Root Mean Square Error	0.46914
Mean of Response	-7.71529
Observations (or Sum Wgts)	67

Analysis of Variance

Source	DF	Sum of Squares	Mean Square	F Ratio
Model	2	40.467216	20.2336	91.9324
Error	64	14.085904	0.2201	Prob > F
C. Total	66	54.553120		<.0001*

Lack Of Fit

Source	DF	Sum of Squares	Mean Square	F Ratio
Lack Of Fit	43	13.154666	0.305922	6.8987
Pure Error	21	0.931238	0.044345	Prob > F
Total Error	64	14.085904		<.0001*
				Max RSq
				0.9829

Parameter Estimates

Term	Estimate	Std Error	t Ratio	Prob>|t|
Intercept	2.6990742	1.556183	1.73	0.0877
1/T, K-1	-2072.15	429.7954	-4.82	<.0001*
pH	-1.013249	0.075378	-13.44	<.0001*

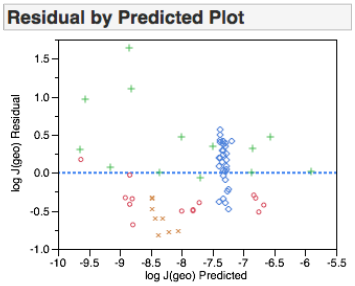

Supplemental Information
Rate equations for modeling carbon dioxide sequestration in basalt
Ryan M. Pollyea & J. Donald Rimstidt
Virginia Polytechnic Institute & State University

Figure S2: JMP output for glassy basalt rates pH > 6.

Source
- Flaathen et al. 2010
- Gislason & Oelkers 2003
- Oelkers & Gislason 2001
- Wolff-Boenisch et al. 2004

Response log J(geo)

Whole Model

Actual by Predicted Plot

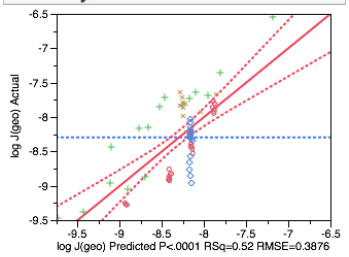

Summary of Fit

RSquare	0.522563
RSquare Adj	0.507407
Root Mean Square Error	0.38758
Mean of Response	-8.29595
Observations (or Sum Wgts)	66

Analysis of Variance

Source	DF	Sum of Squares	Mean Square	F Ratio
Model	2	10.358272	5.17914	34.4773
Error	63	9.463768	0.15022	Prob > F
C. Total	65	19.822039		<.0001*

Lack Of Fit

Source	DF	Sum of Squares	Mean Square	F Ratio
Lack Of Fit	55	9.1176558	0.165776	3.8317
Pure Error	8	0.3461119	0.043264	Prob > F
Total Error	63	9.4637678		0.0243*
				Max RSq
				0.9825

Parameter Estimates

Term	Estimate	Std Error	t Ratio	Prob>|t|
Intercept	-4.278891	0.838846	-5.10	<.0001*
1/T, K-1	-2005.201	288.3978	-6.95	<.0001*
pH	0.2588144	0.036032	7.18	<.0001*

Residual by Predicted Plot

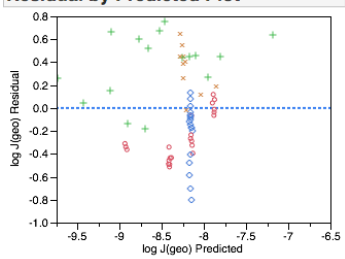

1/T, K-1

Leverage Plot

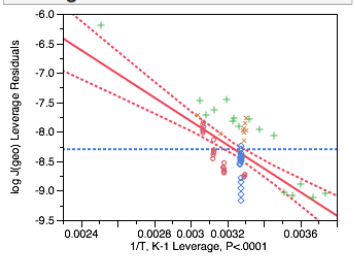

pH

Leverage Plot

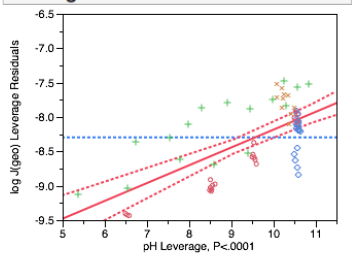

Supplemental Information
Rate equations for modeling carbon dioxide sequestration in basalt
Ryan M. Pollyea & J. Donald Rimstidt
Virginia Polytechnic Institute & State University

Figure S3: JMP output for crystalline basalt rates pH < 6.

Source Data: Gudbrandsson et al. 2011

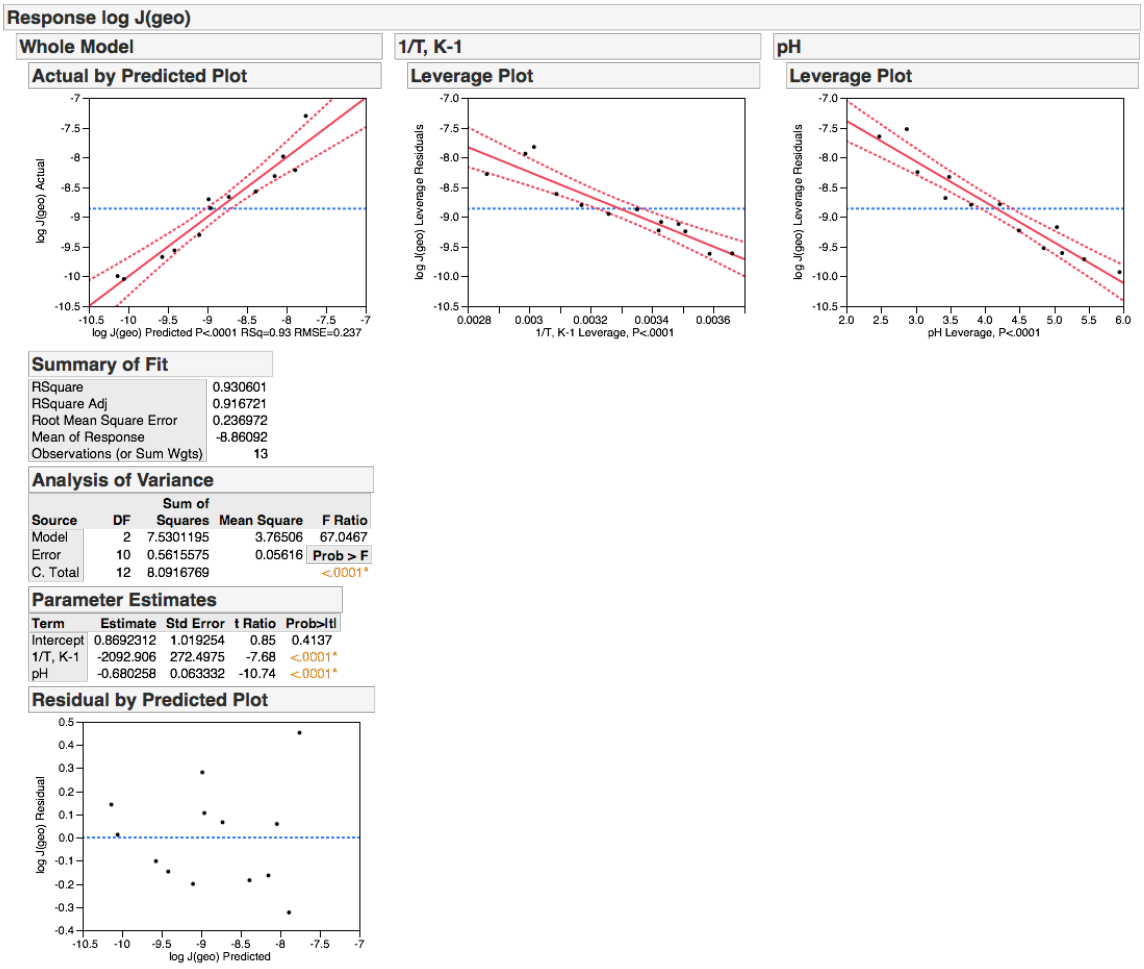

Supplemental Information
Rate equations for modeling carbon dioxide sequestration in basalt
Ryan M. Pollyea & J. Donald Rimstidt
Virginia Polytechnic Institute & State University

Figure S4: JMP output for crystalline basalt rates pH > 6.

Source Data: Gudbrandsson et al. 2011

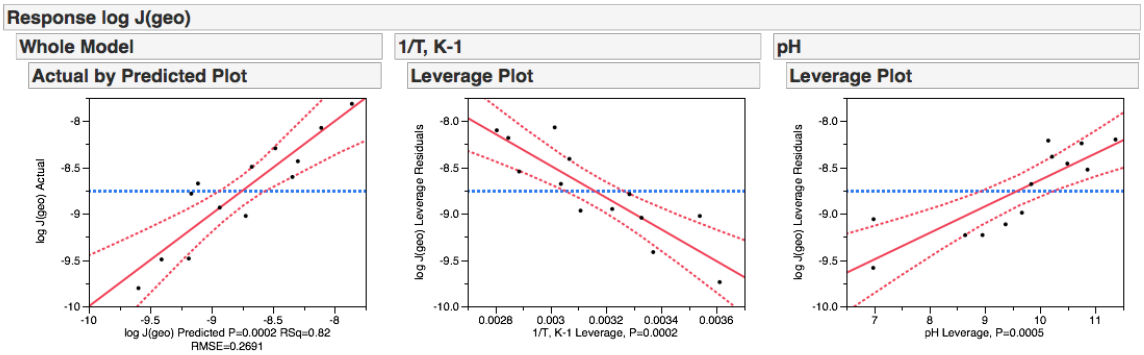

Summary of Fit

RSquare	0.820962
RSquare Adj	0.785155
Root Mean Square Error	0.269103
Mean of Response	-8.76246
Observations (or Sum Wgts)	13

Analysis of Variance

Source	DF	Sum of Squares	Mean Square	F Ratio
Model	2	3.3206031	1.66030	22.9271
Error	10	0.7241661	0.07242	Prob > F
C. Total	12	4.0447692		0.0002*

Parameter Estimates

Term	Estimate	Std Error	t Ratio	Prob>|t|
Intercept	-6.06156	0.977553	-6.20	0.0001*
1/T, K-1	-1719.01	303.8398	-5.66	0.0002*
pH	0.2862616	0.056703	5.05	0.0005*

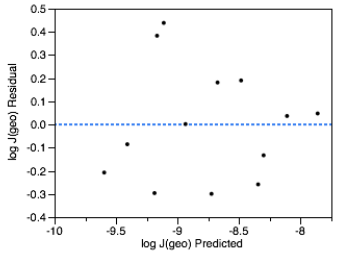

Supplemental Information
Rate equations for modeling carbon dioxide sequestration in basalt
Ryan M. Pollyea & J. Donald Rimstidt
Virginia Polytechnic Institute & State University

Figure S5: Batch reactor simulation results with a sodium-bearing zeolite (Heulandite-Na) included in the alteration product assemblage. A – C illustrate mineral volume fractions for glassy basalt, crystalline basalt, and the composite basalt models, respectively. D – F illustrate aqueous species for glassy basalt, crystalline basalt, and the composite basalt models, respectively.

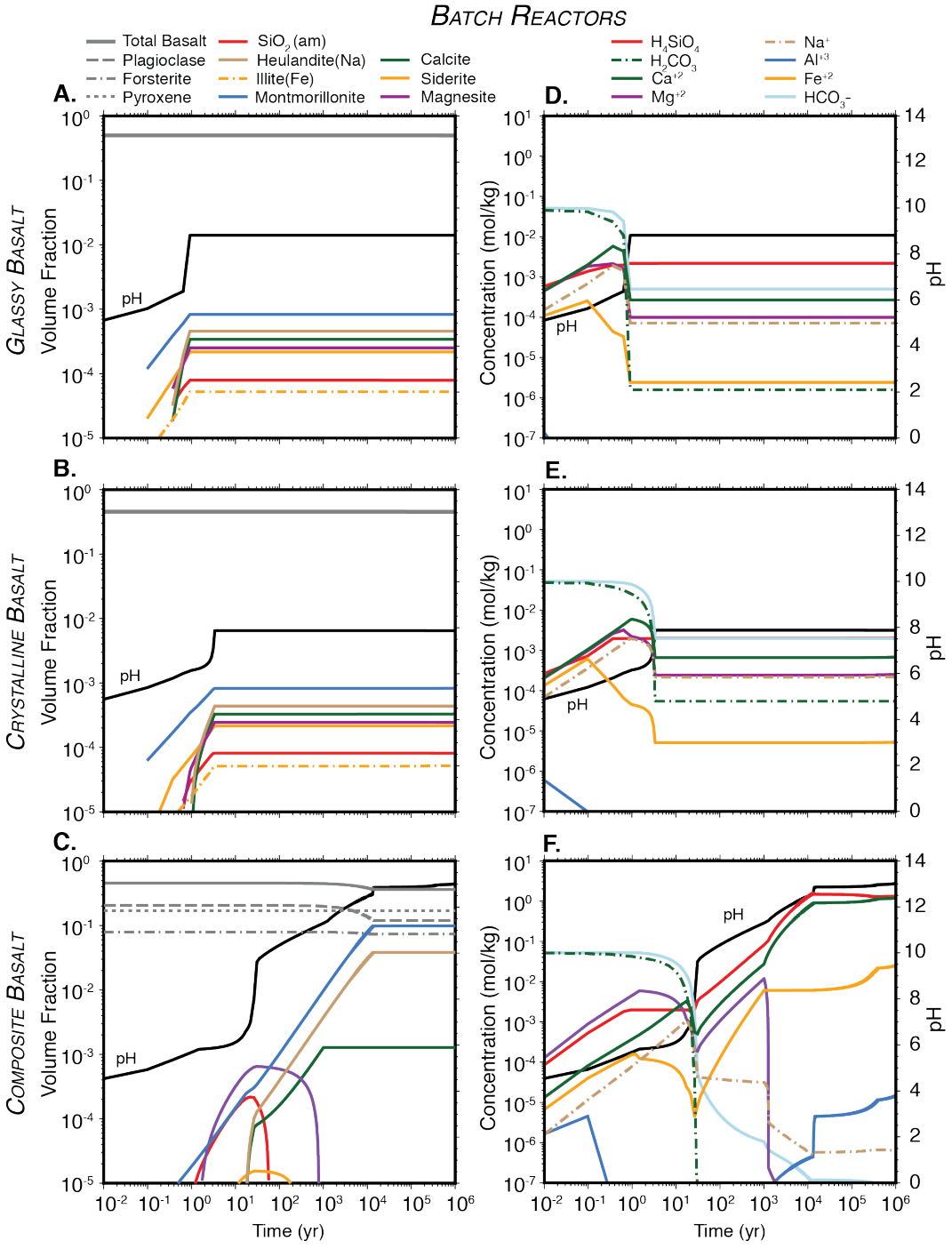

Supplemental Information
Rate equations for modeling carbon dioxide sequestration in basalt
Ryan M. Pollyea & J. Donald Rimstidt
Virginia Polytechnic Institute & State University

Figure S6: Batch reactor simulation results with a sodium-bearing zeolite (Heulandite-Na) included in the alteration product assemblage. A – C illustrate mineral volume fractions for glassy basalt, crystalline basalt, and the composite basalt models, respectively. D – F illustrate aqueous species for glassy basalt, crystalline basalt, and the composite basalt models, respectively.

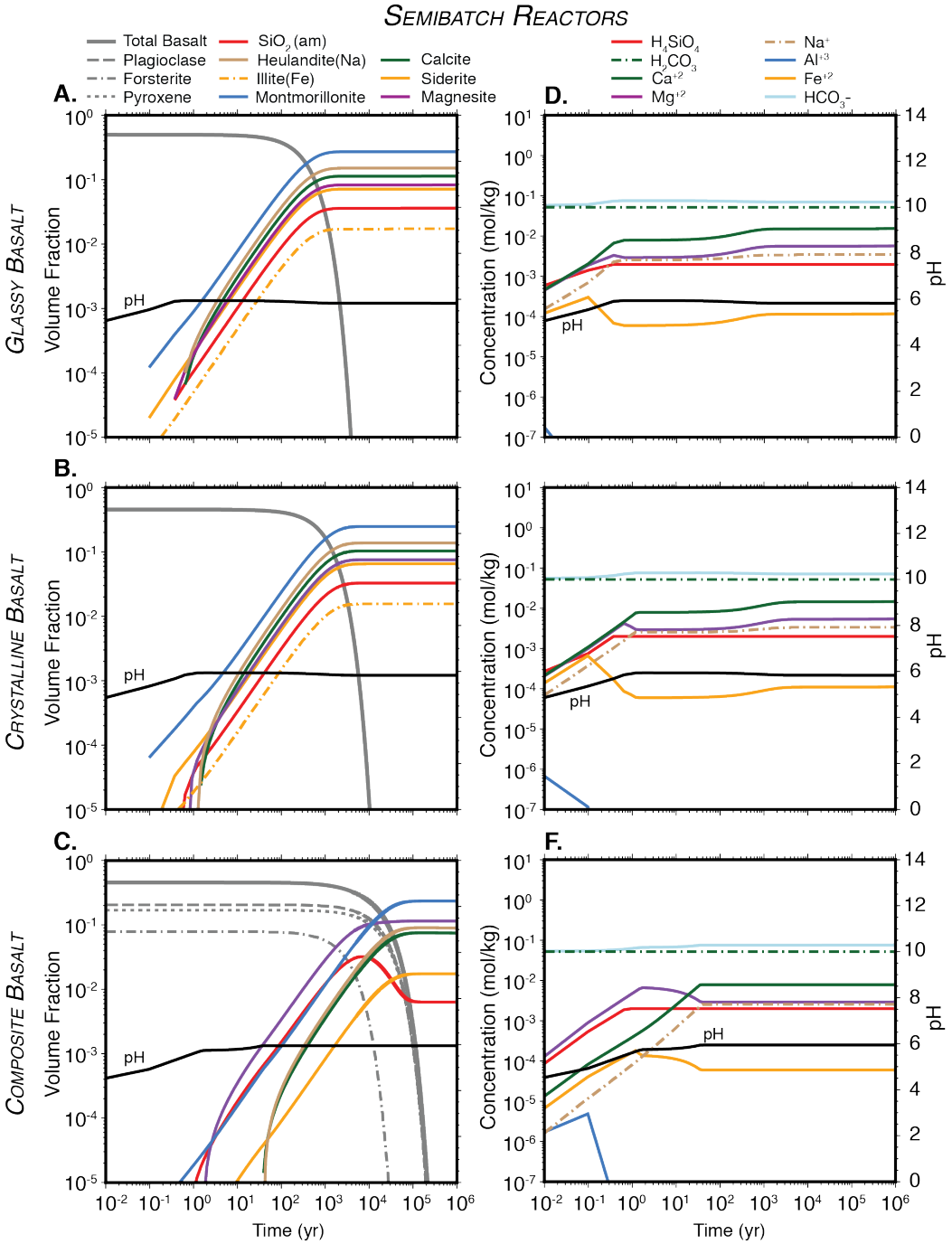

REFERENCES

Flaathen, T.K., Gislason, S.R. and Oelkers, E.H. (2010) The effect of aqueous sulphate on basaltic glass dissolution rates. Chemical Geology 277, 345-354.

Gislason, S.R. and Oelkers, E.H. (2003) Mechanism, rates, and consequences of basaltic glass dissolution: II. An experimental study of the dissolution rates of basaltic glass as a function of pH and temperature. Geochimica et Cosmochimica Acta 67, 3817-3832.

Gudbrandsson, S., Wolff-Boenisch, D., Gislason, S. and Oelkers, E.H. (2011) An experimental study of crysalline basalt dissolution from 2≤pH≤11 and temperatures from 5 to 75°C. Geochimica et Cosmochimica Acta 75, 5496-5509.

Oelkers, E.H. and Gislason, S.R. (2001) The mechanism, rates and consequences of basaltic glass dissolution: I. An experimental study of the disolution rates of basaltic glass as a function of aqueous Al, Si and oxalic acid concentration at 25°C and pH = 3 and 11. Geochimica et Cosmochimica Acta 65, 3671-3681.

Wolff-Boenisch, D., Gislason, S.R., Oelkers, E.H. and Putnis, C.V. (2004) The dissolution rates of natural glasses as a function of their composition at pH 4 and 10.6, and temperatures from 25 to 74°C. Geochimica et Cosmochimica Acta 68, 4843-4858.